Geomechanics and Engineering, *Vol. 34, No. 6 (2023) 649-664*
https://doi.org/10.12989/gae.2023.34.6.649

Sensitivity analysis of mass ratio effect on settlement and seismic response of shallow foundation using numerical simulation

Kil-Wan Ko[1a], Jeong-Gon Ha[2b], Jinsun Lee[3c] and Gye-Chun Cho*[4]

[1]*Department of Civil and Environmental Engineering, University of Southern California, Kaprielian Hall, 3620 South Vermont Avenue, Los Angeles, USA*
[2]*Advanced Structures and Seismic Safety Research Division, Korea Atomic Energy Research Institute, 111 Daedeok Daero 989 beon gil, Yuseong gu, Daejeon, Republic of Korea*
[3]*Department of Civil and Environmental Engineering, Wonkwang University, 460 Iksan-daero, Iksan-si, Jeollabuk-do, Republic of Korea*
[4]*Department of Civil and Environmental Engineering, Korean Advanced Institute for Science and Technology, 291 Daehak-ro, Yuseong-gu, Daejeon, Republic of Korea*

(*Received May 16, 2023, Revised August 12, 2023, Accepted August 13, 2023*)

Abstract. Structural inertial interaction is a representative the effect of dynamic soil–foundation–structure interaction (SFSI), which leads to a relative displacement between soil and foundation, period lengthening, and damping increasing phenomena. However, for a system with a significantly heavy foundation, the dynamic inertia of the foundation influences and interacts with the structural seismic response. The structure-to-foundation mass ratio (*MR*) quantifies the distribution of mass between the structure and foundation for a structure on a shallow foundation. Although both systems exhibit the same vertical factor of safety (FS_v), the *MR* and corresponding seismic responses attributed to the structure and foundation masses may differ. This study explored the influence of *MR* on the permanent deformation and seismic response of soil-foundation-structure system considering SFSI via numerical simulations. Given that numerous dimensionless parameters of SFSI described its influence on the structural seismic response, the parameters, except for *MR* and FS_v, were fixed for the sensitivity analysis. The results demonstrated that the foundation inertia of heavier foundations induced more settlement due to sliding behavior of heavily-loaded systems. Moreover, the structural inertia of heavier structures evidently exhibited foundation rocking behavior, which results in a more elongated natural period of the structure for lightly-loaded systems.

Keywords: dynamic soil-foundation-structure interaction; foundation settlement; inertial behavior; mass ratio; numerical modeling

1. Introduction

Dynamic SFSI demonstrates the effects of each subsystem on the dynamic responses of a superstructure, foundation, and soil. Soil-foundation system transmute from the structural system on a fixed base into a flexible base through the foundation's swaying and rocking responses. Accordingly, the SFSI effects lead to alterations to the dynamic characteristics and responses of the superstructure (Sbartai 2020, Huynh *et al*. 2021, Ngo *et al.* 2019, Stewart *et al.* 1999). The inertial interaction effect demonstrates the phenomena induced by the structural inertial behaviors under dynamic loading. The elongated natural period of the first mode of the soil–foundation–structure (SFS) system and the increase in damping are the consequences of the inertial effect (Ko *et al.* 2021, Trifunac *et al.* 2001, Veletsos and Meek, 1974). The inertial loads applied to the superstructure cause relative deformations between the soil and foundation, thereby leading to permanent deformations, such as settlement, tilting, and sliding (Wolf 1985). To simplify the SFS system, SFSI effects delineate the SFS system as an equivalent single-degree-of-freedom (SDOF) structure with the swaying and rocking springs and dashpots of the foundation (Chen *et al.* 2013, Martakis *et al*. 2017).

Kinematic interaction elucidates a foundation input motion that is different from a free-field soil response due to base slab averaging, wave scattering, and impedance differences between the soil and the foundation (Stewart 2000). Although the kinematic interaction only considers the foundation as a modulator of the input wave characteristics for SFSI problems, the inertia of the foundation can influence the SFSI effects and permanent deformation after shaking, and interact with the structural inertial effect (Safak 1995, Ko *et al*. 2020). The structure-to-foundation mass ratio (*MR*) (i.e., structural mass divided by foundation mass) is a dimensionless parameter that represents the inertia of the foundation and structure (Ha *et al.* 2019, Veletsos and Meek 1974). Moreover, the dimensionless parameters with respect to the SFSI (i.e., structural aspect ratio, soil-to-structure stiffness ratio, and structure-to-soil mass ratio) are correlated to such an extent that they limit the isolation and investigation of the effects of each parameter.

*Corresponding author, Professor
E-mail: gyechun@kaist.ac.kr
[a]Postdoctoral Researcher
[b]Senior Researcher
[c]Professor

ISSN: 2005-307X (Print), 2092-6219 (Online)

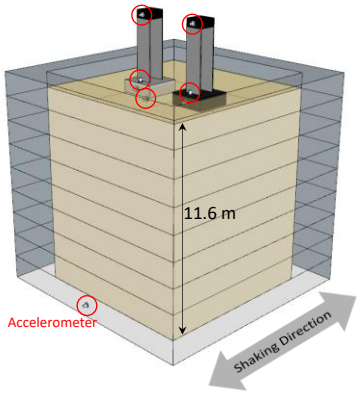

(a) 3D view

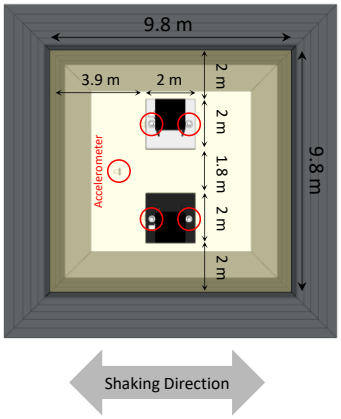

(b) Plan view (Ko *et al.* 2020)

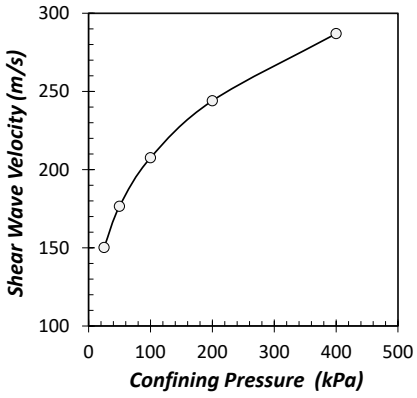

(c) Shear wave velocity of silica sand

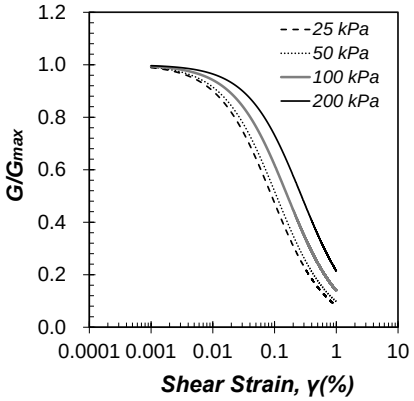

(d) Shear modulus degradation curves of silica sand

Fig. 1 Centrifuge test model with two SDOF structures on shallow foundations using the dry silica sand

In the static and seismic design of a shallow foundation, the vertical factor of safety (FS_v) of the foundation (i.e., the ratio of the bearing capacity of the foundation to the dead load from the structure and foundation's masses) is widely employed as a key design parameter. Given that the FS_v determines the position of the plastic "hinging" in the superstructure or in the soil–foundation system (Anastasopoulos *et al.* 2010, Deviprasad and Dodagoudar 2020), the energy dissipation mechanism of the SFS system and structural seismic responses significantly depend on the FS_v (Kim *et al.* 2015). For the given soil properties, applied vertical load, and foundation dimension, i.e., if both systems have the same FS_v, the *MR* attributed to the structure and foundation masses can differ. Accordingly, it is necessary to evaluate the influences of the *MR* on the seismic responses of the structure and on the dynamic performance of the foundation, which include nonlinear-plastic responses, such as rocking, swaying, and permanent settlement.

The numerical modeling of the SFSI problems determines the mechanical properties of the SFS system; thus, it is useful to separately evaluate the effects of each dimensionless parameter on the seismic responses of the foundation and structure. Previous studies (Lee *et al.* 2015, Tabatabaiefar and Fatahi 2014, Yoo *et al.* 2022) confirmed the validity of the interface models in FLAC3D by comparing the results with centrifuge test results. Hence, in this study, the three-dimensional (3D) finite-difference program FLAC3D was applied to the shallow footing SFSI problems.

This study aims at investigating the effects of the *MR* on the seismic responses of the foundation, structure, and the permanent deformation in the foundation. Numerical analyses were performed on a SDOF structure on a shallow foundation with a dry sand layer. The centrifuge test results pertaining to the SFSI studies validated the established numerical model. The *MR* and FS_v were varied by maintaining the other dimensionless parameters, such as the structural aspect ratio, soil-to-structure stiffness ratio, and structure-to-soil mass ratio. The SFSI effect on structural seismic acceleration was discussed, and foundation settlement, rocking, and sliding mechanisms were evaluated in terms of the *MR*. Moreover, the plastic deformation, damping ratio, and foundation stiffness degradation were discussed with respect to the system *MR* and FS_v based on the moment–rotation and shear force-sliding hysteresis loops.

2. Dynamic centrifuge test

In this study, the dynamic centrifuge test performed by Ko *et al.* (2020) was selected to validate the numerical model. The centrifuge test was performed using the beam-type centrifuge facility at KAIST Analysis Center for Research Advancement (KARA). The centrifugal

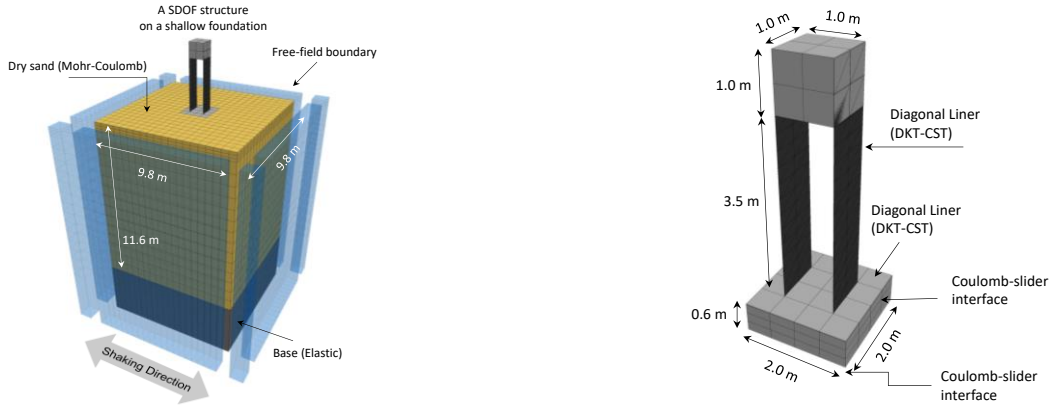

(a) Soil-foundation-structure model (b) Foundation-structure system

Fig. 2 Finite difference model for numerical analysis

acceleration was a 20 g-level, and the model dimensions and properties were expressed on the prototype scale (Fig. 1) by applying the centrifuge scaling law (Schofield 1980). Ko *et al.* (2020) provided detailed information on the centrifuge tests.

For the centrifuge test, an equivalent shear beam (ESB) container was used with dimensions of 49 × 49 × 63 cm^3 on the model scale and 9.8 × 9.8 × 11.6 m^3 on the prototype scale (length × width × height, respectively). The ESB container reduces the boundary effect between the soil and adjacent wall during shaking when the soil fully occupies the container (Lee *et al.* 2013). The dry pluviation method was used to reconstitute the ground model into an ESB box using silica sand with a relative density of 60%. Silica sand was artificially manufactured via a hammer crusher process. The Unified Soil Classification System (USCS) classifies silica sand as poorly graded sand (SP). Resonant column (RC) and torsional shear tests (TS) were conducted to derive a relationship between the shear wave velocity of soil (V_s) and confining pressure, in addition to the shear modulus degradation curves of silica sand with a relative density of 60 % corresponding to dry density of 1.46 t/m^3 (Figs. 1(c) and 1(d)). The soil properties at the 20 g-level are as follows: internal friction and dilation angle are 40.9° and 10.9°, respectively, and Poisson's ratio is 0.26.

The structural model consisted of a lumped mass supported by two thin steel columns to simulate the SDOF structure. The dimensions of the lumped mass were 1 × 1 × 0.2 m^3 (length × width × height, respectively), and the height of the two thin steel columns was 3.5 m. Impact hammer tests were conducted to determine the natural frequencies of the structure model, which was 3.72 Hz (0.27 s).

Two square foundation models were used to represent the light- and heavy-weight foundations fabricated using aluminum and steel, respectively. The foundation dimensions were 2 × 2 × 0.6 m^3 (length × width × height, respectively), and the models were fully embedded with an embedment depth of 0.6 m. This study only simulated the heavy foundation model. The bearing capacities of the foundation were calculated using the Meyerhof's (1963) equation. The estimated FS_v of the model with the heavy foundation and the structural model was 39.51, which was excessively high to reflect the effect of FS_v on the dynamic SFSI response. Hence, to design a lower FS_v system, the structural dimensions and volume of the lumped mass were intentionally extended after validating the numerical model with the centrifuge test results.

Four accelerometers were attached to the foundation structure model as follows. Two accelerometers were installed vertically on the foundation to measure the rocking responses. The other two accelerometers were installed at the lumped mass and foundation to measure the horizontal seismic responses of the structure and foundation. In addition, two accelerometers were installed at the bottom of the ESB box and the soil surface to measure the input motion of the numerical analysis and the free-field soil surface motion of the soil. The input motions for the centrifuge tests were records of the Hachinohe and Ofunato earthquakes from the $\boldsymbol{M}_{\mathrm{w}}$7.9 Tokachi-Oki earthquake that occurred on May 16, 1968 and the $\boldsymbol{M}_{\mathrm{w}}$7.4 Miyagi-Ken Oki earthquake that occurred on June 12, 1978. In particular, these represent long-period- and short-period-dominated earthquake signals, respectively. The frequency contents of the recorded earthquake were filtered with respect to the loading frequency range of the shaking table, which was 40–300 Hz for random vibration waves. At the early stage, strong earthquake signals from the Ofunato and Hachinohe earthquakes were applied to the model. Subsequently, the input intensities of the signals increased in stages. Given that the stage tests could not retain the initial conditions of the SFS system, the numerical model was validated using the centrifuge test results when a strong earthquake was applied as an initial input motion.

3. Numerical analysis for SFSI

The three-dimensional (3D) finite-difference method (FDM) program FLAC 3D (Itasca Consulting Group, 2019) was adopted to conduct nonlinear time-domain dynamic analyses using an explicit method. The numerical model was solved in accordance with the centrifuge model setup procedure to reflect the soil behaviors with respect to their stress history.

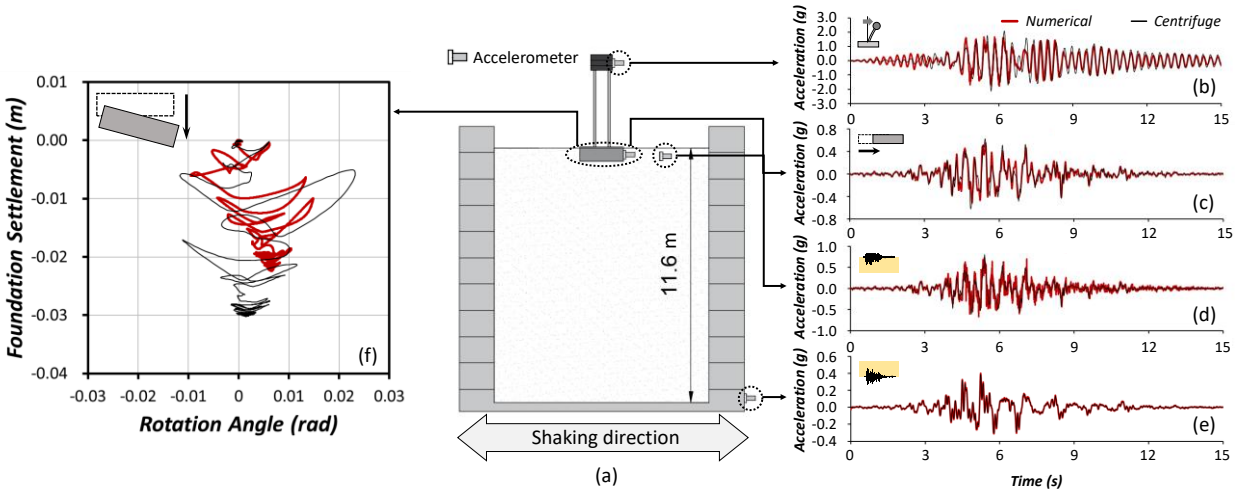

Fig. 3 Comparison between the dynamic responses of soil, foundation, and structure system between the centrifuge test and the numerical analysis (Hachinohe, input peak acceleration: 0.38 g): (a) schematic of the centrifuge test model; acceleration time histories (Ko *et al.* 2021), (b) structural responses, (c) foundation horizontal responses, (d) soil free-field responses, (e) input motions and (f) rotation-settlement responses of the foundation

The dimensions of the numerical models coincided with those of the centrifuge model on the prototype scale, at the 20 g-level (Fig. 2). The element of the model was a hexahedron grid, and the maximum size of the elements was determined based on the Lysmer and Roger's (1969) equation, as follows.

$$\Delta l \leq \frac{\lambda}{10} = \frac{V_s}{10 \times f} \quad (1)$$

where Δl is the element size; and λ and f are the wavelength and frequency corresponding to the highest frequency energies in the applied dynamic input wave, respectively. The maximum input frequency of the shaking table for the centrifuge test was 15 Hz at the prototype scale, and the minimum V_s of the soil model was 80 m/s at the soil surface. Hence, Δl for the numerical model associated with the maximum element size should be less than 0.53 m. The applied free-field boundaries at each corner suppressed the wave reflection at the side of the model.

3.1 Ground model and boundary condition

The dimensions of the ground model were 9.8 × 9.8 × 11.6 m^3 (length × width × height, respectively) corresponding to the centrifuge model. V_s of the soil within a small strain range is a function of the confining stress applied to the soil. To induce a variation in V_s with respect to the depth of the soil layer, an elastic model for the silica sand was initially assigned to the soil properties, as presented in Table 1. After the first static equilibrium condition, the soil model was changed to the Mohr–Coulomb model, and the initial shear and bulk modulus of the silica sand were updated based on the V_s-confining stress relationship (Fig. 1(c)).

A hyperbolic model was used to simulate the cyclic nonlinearity of the soil depending on the strain level before plastic failure (Hardin and Drnevich 1972). The fitting curves of the shear modulus degradation (Fig. 1(d)) were applied to the soil model in accordance with the confining stress at each layer and frequency-independent hysteretic damping was in accordance with the applied fitting curves. Rayleigh damping, which is frequency-dependent damping, was employed to determine the minimum damping of the soil at small strains and reduce the high-frequency noise of the dynamic responses. FLAC 3D requires a fraction of the critical damping and center frequency for Rayleigh damping. Herein, the critical damping was 0.01, and the center frequency was set as 4.5 Hz, as associated with the fundamental frequency of the soil deposit (Sun and Dias 2018).

The bottom of the ESB box was modeled as an elastic model based on the mechanical properties of aluminum. The critical dynamic time step for explicit analysis is predominantly governed by elements with sizes smaller than that of the other elements, and with a relatively larger stiffness. Accordingly, the size of the base elements simulating the ESB box was intentionally extended to reduce the computational time. A quiet boundary, which was based on the use of independent dashpots, was applied at the model base to represent a compliant base (Mejía and Dawson 2006).

3.2 Numerical modelling for foundation and structure model

The foundation model was fully embedded, and the dimensions of the model were the same as those of the centrifuge model. The model was located at the center of the numerical model (Fig. 2(a)). The foundation model should possess adequate interfaces that enable sliding or separation. Therefore, the interfaces between the foundation and soil model were generated on the zone faces with Coulomb-slider interfaces. The *bonded-slip* command allows slip between the interfaces even for high strain range during the shaking. The interfaces consisted of a linear spring (K_n) in the normal direction without tensile resistance and a spring-slider (K_s) in the shear direction (Lee *et al.* 2015). The apparent stiffnesses of the interface model for stable numerical integration can be

Table 2 Properties of interface model

Properties	Value
Subgrade reaction stiffness in normal direction, K_n (GPa/m)	1.22
Subgrade reaction stiffness in shear direction, K_s (GPa/m)	1.22
Cohesion (Pa)	0
Interface friction angle (°)	30

calculated as (Itasca Consulting Group 2019)

$$K_s = K_n = 10 \times \max\left[\frac{K + \frac{4}{3}G}{\Delta z_{min}}\right] \quad (2)$$

where K and G are the bulk and shear moduli within a small strain range of adjacent soil elements, respectively; and Δz is the smallest width of the adjoining zone in the normal direction. After installation of the foundation model and static analysis, K and G were obtained from adjacent soil elements. In order to accurately simulate the permanent deformation of the foundation attributed to its sliding and rocking, the mesh size, Δz_{min}, for the soil elements close to the foundation was reduced by three times compared to the other soil elements. The estimated K_n, K_s, and other interface properties are listed in Table 2.

The structural model comprised a lumped mass, which was located at the top, and two structural columns (Fig. 2(b)). To increase the structural weight for the *MR*, the dimensions of the lumped mass were extended for the parametric analysis, unlike the centrifuge model. Solid and shell elements were used to design the lumped mass and two structural columns, respectively. The discrete Kirchhoff triangle-constant strain triangle (DKT-CST) of the shell elements was used to simulate the flexural response of the structure. The Poisson ratio and thickness of the shell elements were 0.3 and 0.2 m, respectively, corresponding to the centrifuge structure model. Given that Rayleigh damping can significantly lengthen the analysis time, a combined local damping of 0.5% was assigned to the structure and foundation model.

3.3 Validation of numerical models based on centrifuge test

The acceleration time histories of the input motion, free-field, foundation-horizontal, and structural responses along with the foundation rotation–settlement responses obtained from the centrifuge and numerical results were compared (Fig. 3). The horizontal acceleration responses of the soil, foundation, and structure model from the numerical model were in good agreement with those of the centrifuge tests, irrespective of the model locations (Figs. 3(b)-3(e)). The foundation settlement of the centrifuge test reached 1.5% of foundation length (L), whereas that of the numerical analysis was close to 1.1% of L (Fig. 3(f)). Compared with the centrifuge model, the foundation of the numerical model exhibited a lower peak rotation angle during an earthquake. Given that the soil at the surface was generally under less confining stress in centrifuge tests, the V_s decreased at the soil surface, which was reconstituted by the pluvation method (Lee *et al.* 2013), and the permanent settlement of the centrifuge test was larger than that of the numerical settlement. The settlement in the centrifuge test occurred due to the reduction of the particle void, whereas permanent settlement in the numerical model using the Mohr–Coulomb model occurred due to the local bearing capacity failure. However, the difference between these deformations was negligible.

3.4 Parameter selection for the sensitivity analysis

3.4.1 Foundation–structure properties for numerical analysis

The independent variables were the *MR* and FS_v, which were used to investigate the effect of the *MR* on the dynamic response of the foundation–structure system by varying the FS_v of the system. In most design guidelines for shallow foundations, $FS_v = 3$ is a static design criterion (Cheney and Chassie 2000, Kimmerling *et al.* 2002). Gajan and Kutter (2008) proposed $FS_v = 10$ as an optimized design that achieves a tradeoff between permanent deformation and energy dissipation via the ground. The FS_v of the constructed shallow foundation for bridges are within the range of 9–24 (Shirato *et al.* 2008). Correspondingly, FS_v was set as 3, 10, 24. Moreover, the *MR* values from the database of rocking shallow foundations based on dynamic centrifuge tests are within the range of 2–18 (Gavras *et al.* 2020). Therefore, *MR* was set as 2, 10, and 18. The nine foundation-structure models were labeled in accordance with their FS_v and *MR* values. For example, FS3_MR2 indicates a system with $FS_v = 3$ and $MR = 2$. The properties of the foundation structural model are listed in Table 3.

The dimensionless parameters, structural aspect ratio, and soil-to-structure stiffness ratio were the control variables. The control variables are associated with the physical dimensions of the foundation-structure system, structural natural frequency (f_n), and V_s of the soil. The structural aspect h/L (i.e., structural height h divided by L) was fixed as 2.3, thus indicating a rocking-dominated system response instead of sliding (Gajan and Kutter 2009).

The soil-to-structure stiffness ratio ($\sigma = V_s/f_n h$) is a function of V_s of the soil and f_n. Soil properties are constant regardless of the foundation structure system whereas f_n is interdependent on the structural mass and stiffness (k_s). To maintain f_n for each foundation-structural model by altering the structural mass, k_s should be modified using the corresponding elastic moduli of the structural columns.

The free vibration characteristics of the nine structural models were investigated to validate f_n. Nine structural models, which did not reflect the SFSI effects, were designed under the fixed–base condition. The Ormsby wavelet features a controllable flat frequency content, which allows for the investigation of f_n of the structure (Fig. 4(a)). The free vibration of the structure in the time domain under the Ormsby wavelet reveals the vibration characteristics of the structure (Fig. 4(a)). The nine model ratios of the ratio of response spectrum (RRS) between the input motion and structural response exhibited the $f_n = 2.5$ Hz for the structure models (Fig. 4(c)) as obtained from the acceleration responses spectrum (Fig. 4(b)).

Table 3 Foundation and structure models for numerical analysis

Parameters									
FS_v	3	3	3	10	10	10	24	24	24
MR	2	10	18	2	10	18	2	10	18
Name of models	FS3_MR2	FS3_MR10	FS3_MR18	FS10_MR2	FS10_MR10	FS10_MR18	FS24_MR2	FS24_MR10	FS24_MR18
m_f (kg)	77975	21265	12311	23392	6379	3693	9746	2658	1538
Foundation density (kg/m^3)	29535	8055	4663	9845	2685	1554	3691	1006	582
Structural mass (kg)	155950	212659	221613	46785	63797	66483	19493	26582	27701
m_s (kg)	148152	202027	210534	44448	60611	63164	17271	23551	24543
k_s (kN/m)	38.5	52.5	54.7	11.5	15.7	16.4	4.8	6.6	6.8
Structural density (kg/m^3)	55696	75949	79147	16708	22784	23744	6962	9493	9893
h (m)	4.6	4.6	4.6	4.6	4.6	4.6	4.6	4.6	4.6
Elastic modulus of structural column (GPa)	384	523	545	115	157	163	45	61	64
f_n (Hz)	2.5	2.5	2.5	2.5	2.5	2.5	2.5	2.5	2.5

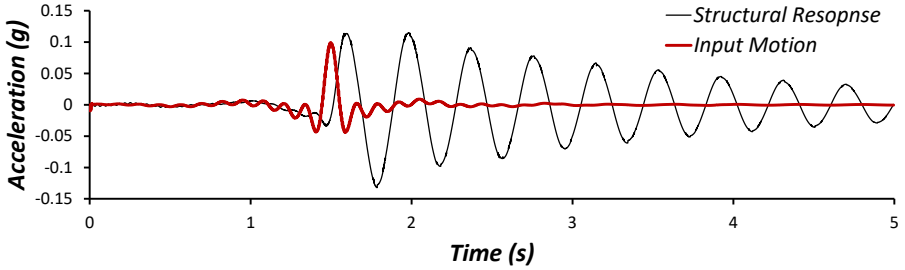

(a) Acceleration time histories of input motion and structural response

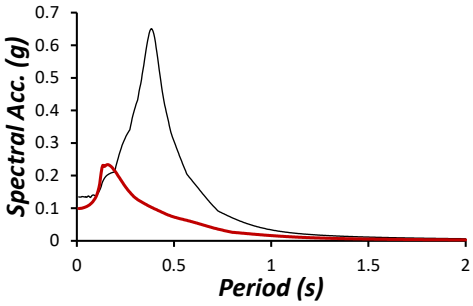

(b) Acceleration response spectrum

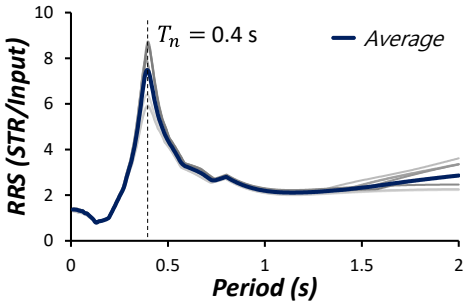

(c) RRS between the structure and input motion for the nine foundation-structure models

Fig. 4 Structural response under Ormsby wavelet

3.4.2 Input motions

The numerical models utilized the Hachinohe and Ofunato earthquake records as the input motions (Fig. 5). The frequency bands of both input motions included 2.5 Hz, which was the f_n of the structure models. The peak accelerations of the input motion were 0.05, 0.15, and 0.35 g, which correspond to weak, moderate, and strong earthquakes, respectively. Unlike centrifuge tests, a numerical analysis can determine the effect of the *MR* on the SFS system without interfering with the model due to the stage tests that input multiple seismic waves to a model. The nine foundation–structure models, two input motions, and three input peak accelerations resulted in 54 cases for the sensitivity study.

4. Evaluation of *MR* effects on SFSI responses and permanent deformation from numerical parametric analysis

4.1 SFSI effects on the system seismic acceleration responses

The SFSI effects were investigated by comparing the seismic structure response from the numerical analysis with the fixed condition from the analytical calculations. The seismic acceleration ($\ddot{u}_{net}$) of the SDOF under fixed base conditions was estimated using the following equation.

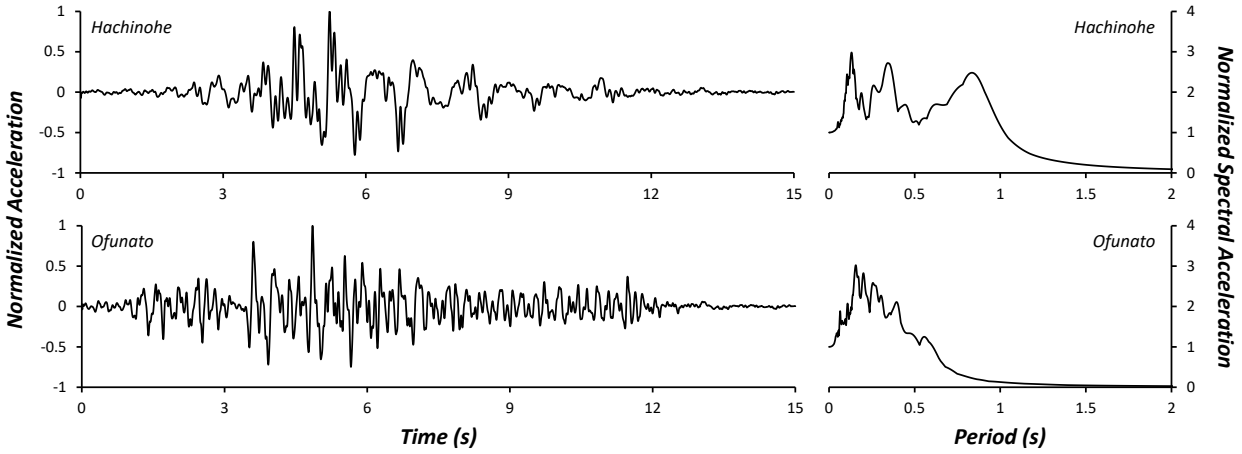

Fig. 5 Acceleration time-histories and response spectrums of input motions, Hachinohe and Ofunato earthquake records

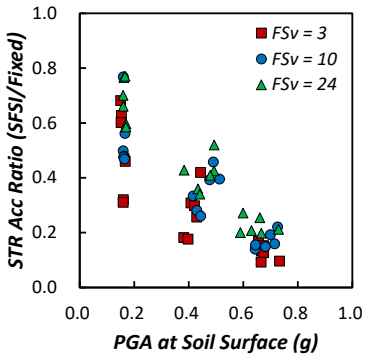

(a) Acceleration ratio of the structure responses from numerical results to that on the fixed base condition with peak ground acceleration at soil surface

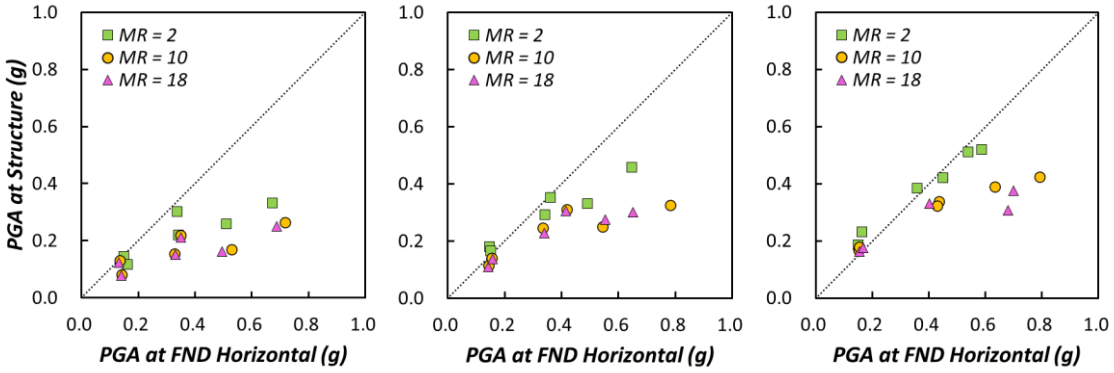

(b) FS_v = 3 (c) FS_v = 10 (d) FS_v = 24

Fig. 6 Peak acceleration responses of soil, foundation, and structure considering the SFSI effects

$$m_s\ddot{u}_{net} + c_s\dot{u}_{net} + k_s u_{net} = -m_s\ddot{u}_g \quad (3)$$

where m_s is the structural effective mass; c_s and k_s are the structural damping coefficient and stiffness, respectively; and $\ddot{u}_g$ is the acceleration response of the free-field soil surface. The structural damping ratio was assumed to be 8%, and the m_s and k_s values are listed in Table 3. The $\ddot{u}_g$ was obtained from the numerical analysis.

The structural acceleration ratios (i.e., the structure acceleration considering SFSI to the structure acceleration under fixed-base conditions) were less than unity, thus indicating that the SFSI effects were completely beneficial for the models in this study (Fig. 6(a)). The larger peak ground acceleration (PGA) at the soil surface, the less acceleration ratio. The foundation dynamic behavior was further promoted, and the structural seismic demand decreased with an increase in the seismic intensity of the ground surface.

As FS_v decreased, the significance of the reduction in the peak acceleration of the structure increased, as compared with the foundation response (Figs. 6(b)-6(d)). Heavily-loaded

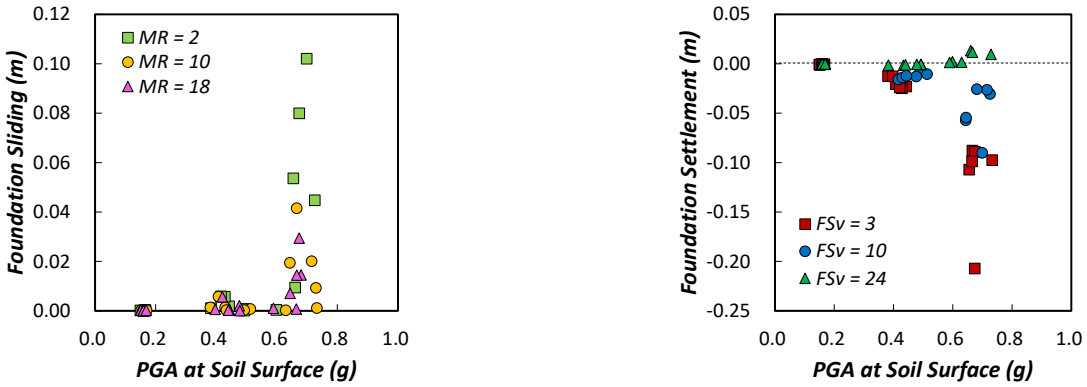

(a) Sliding (b) Settlement

Fig. 7 Permanent deformation of the foundation with peak ground acceleration at soil surface

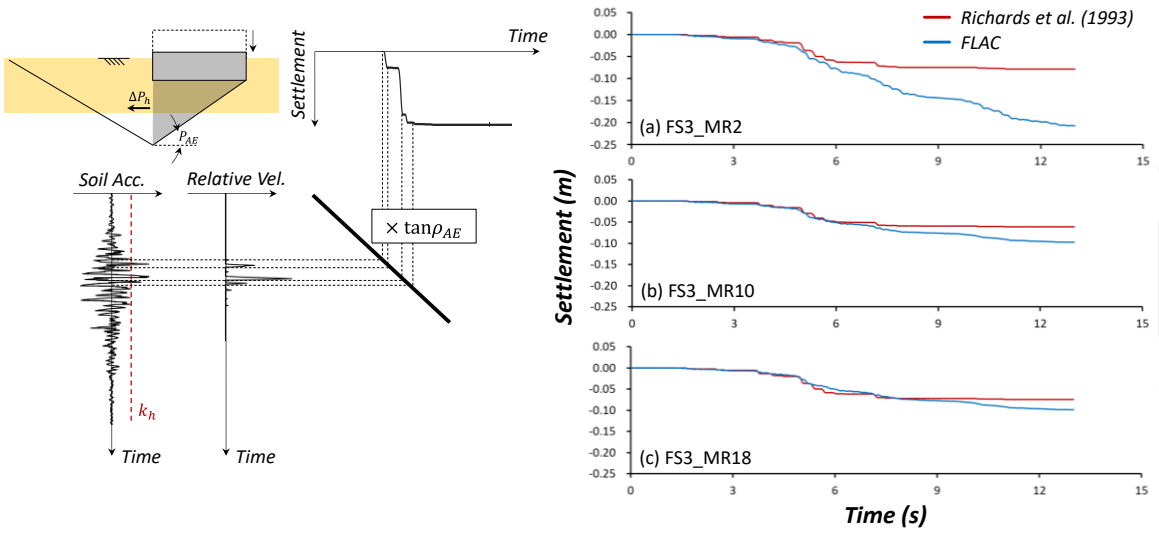

Fig. 8 Comparison foundation settlement time histories between the numerical analysis and the analytical estimation under the strong shaking (Ofunato, PGA at free-field soil surface: 0.78 g): (a) FS3_MR2, (b) FS3_MR10 and (c) FS3_MR18

systems (lower FS_v), which dissipate more seismic energy via the soil–foundation system instead of the structure, have more significant effects on the SFSI as compared with the lightly-loaded system (higher FS_v). The rocking effect of shallow footing reduces the structural response due to the ultimate moment capacity of the foundation, which decreases with FS_v (Gajan *et al.* 2005). Moreover, the maximum seismic acceleration is limited through the relation between the overturning moment of the foundation attributed to the structural seismic acceleration and the ultimate moment capacity, which is called rocking effect. The structural seismic acceleration inversely proportional to the mass of the superstructure (Kim *et al.* 2015). Accordingly, for the same FS_v systems, the systems with lower *MRs* (lighter structure with a heavier foundation) exhibited relatively higher seismic responses of the structure.

4.2 Permanent deformation of the foundation: sliding and settlement

The permanent settlement of the foundation increased with the PGA at the soil surface (Fig. 7). Heavily-loaded systems achieve settlement more readily than lightly-loaded systems, which shift upward when the PGA at the soil surface is larger than 0.6 g (Fig. 7(b)). The permanent sliding of the foundation does not significantly occur when the PGA is less than 0.6 g (Fig. 7(a)). However, the effect of *MR* on sliding becomes clear when PGA is larger than 0.6 g; heavier foundations (the lower *MR*) slide more readily than lighter foundations under strong shaking. The foundation inertia leads to more sliding, as detailed in the following section.

4.3 Effect of MR for heavily-loaded systems: FS_v = 3

4.3.1 Foundation settlement

A reduction in the bearing capacity of the foundation leads to a gradual accumulation of the settlements of shallow foundations under a strong earthquake. Richards *et al.* (1993) applied the Newmark sliding block method (Newmark 1965) to analytically estimate the foundation seismic settlement. The active wedge angle of the simplified static slip field with Coulomb wedges is P_{AE}, and the seismic acceleration induces an additional passive pressure (ΔP_h) on the wedges (Fig. 8).

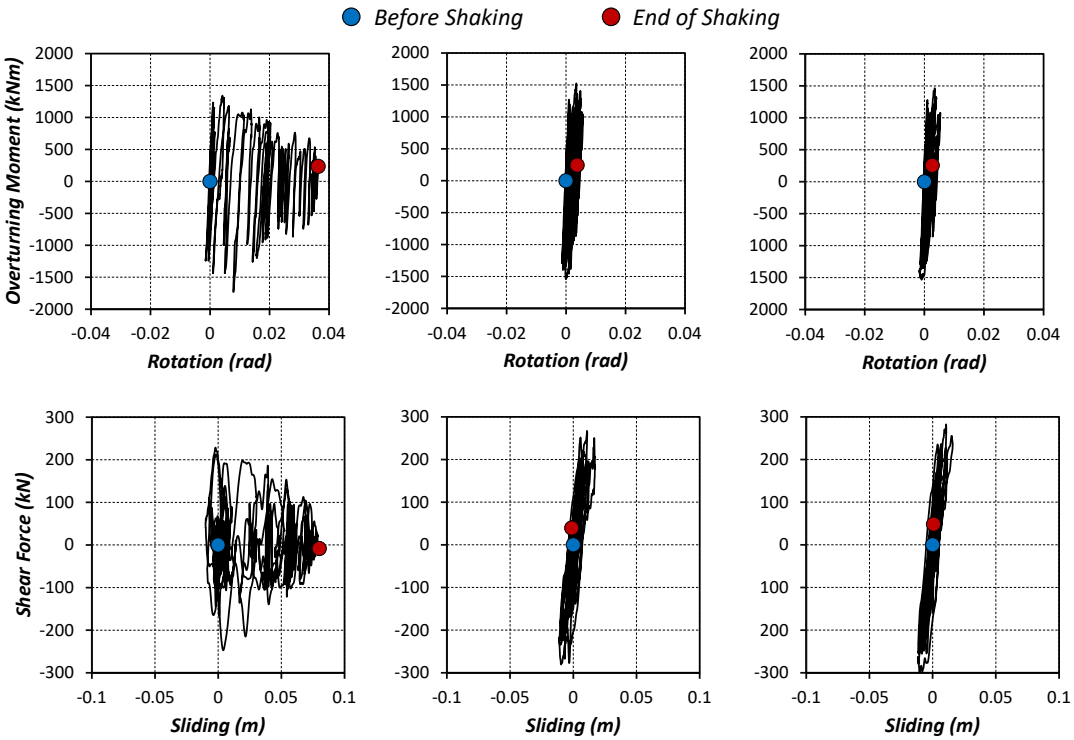

(a) FS3_MR2 (b) FS3_MR10 (c) FS3_MR18

Fig. 9 Moment-rotation and shear force-sliding responses of the foundation with FS_v=3 under the strong shaking (Ofunato, PGA at free-field soil surface: 0.78 g)

The critical acceleration (k_h) is calculated based on FS_v, the friction angle of the soil, the embedment depth of the foundation, and P_{AE}. If the foundation horizontal acceleration exceeds the k_h, foundation settlement occurs at the value associated with the relative velocity between the foundation and k_h.

The foundation settlements of the system with $FS_v = 3$ obtained from the numerical analysis were compared with those obtained from the analytical estimation by Richards *et al.* (1993). The analytical estimation reasonably predicted the settlements from the numerical analysis for the MR10 and MR18 cases (Figs. 8(b) and 8(c), respectively). This indicates that the settlement mechanisms of the MR10 and MR18 cases can be attributed primarily to the seismic bearing capacity failure. However, there was a significant difference between the numerical and analytical settlements for the heavier foundation (MR2) (Fig. 8(a)). This phenomenon can be expressed by foundation rocking and sliding responses, instead of the bearing capacity failure.

4.3.2 Foundation rocking and sliding responses

The overturning moment–rotation and shear force-sliding responses of the foundation intuitively demonstrate the nonlinear-plastic behavior of the foundation under the earthquake (Fig. 9). The overturning moment (M_o) and shear force (F_h) applied to the foundation are calculated as

$$M_o = m_s h \ddot{u}_s, \tag{4}$$

$$F_h = m_s \ddot{u}_s + m_f \ddot{u}_f, \tag{5}$$

where $\ddot{u}_s$ and $\ddot{u}_f$ are the measured accelerations at the structure and foundation, respectively; and m_f is the mass of the foundation.

As expected, sliding and permanent tilting due to rocking occurred primarily in FS3_MR2, and plastic deformations accumulated when the M_o and F_h were reached at the maximum value of each cycle. The permanent sliding and rotation of FS3_MR2 were 4% of L and 17% of the toppling rotation angle; whereas the permanent rotations of FS3_MR10 and FS3_MR18 were less than 2.8% of the toppling rotation angle, and permanent sliding was negligible in both cases. The hysteretic responses of the shear force–sliding for FS3_MR10 and FS3_MR18 exhibited closed loops of hysteresis, and yielding occurred at the maximum F_h.

To obtain the hysteretic damping ratio and nonlinear stiffness from the overturning moment–rotation and shear force-sliding responses, the hysteresis loops were derived from the double integration of the acceleration signals, which did not measure the permanent sliding and rotation. Numerous cyclic responses from the hysteresis loops were divided into cycles under a strong earthquake. The methods used to estimate the plastic deformation, damping ratio, and nonlinear stiffness for each cycle are illustrated in Fig. 10. Given that the maximum M_o, F_h, and permanent deformation did not occur simultaneously, each maximum value was obtained from the averaged absolute values of the maximum and minimum values. Plastic deformation corresponds to deformation when the M_o and F_h reach zero in the hysteresis loop.

Fig. 10 depicts the plastic deformation, damping ratio, and nonlinear stiffness for each cycle of FS3_MR2, FS3_MR10,

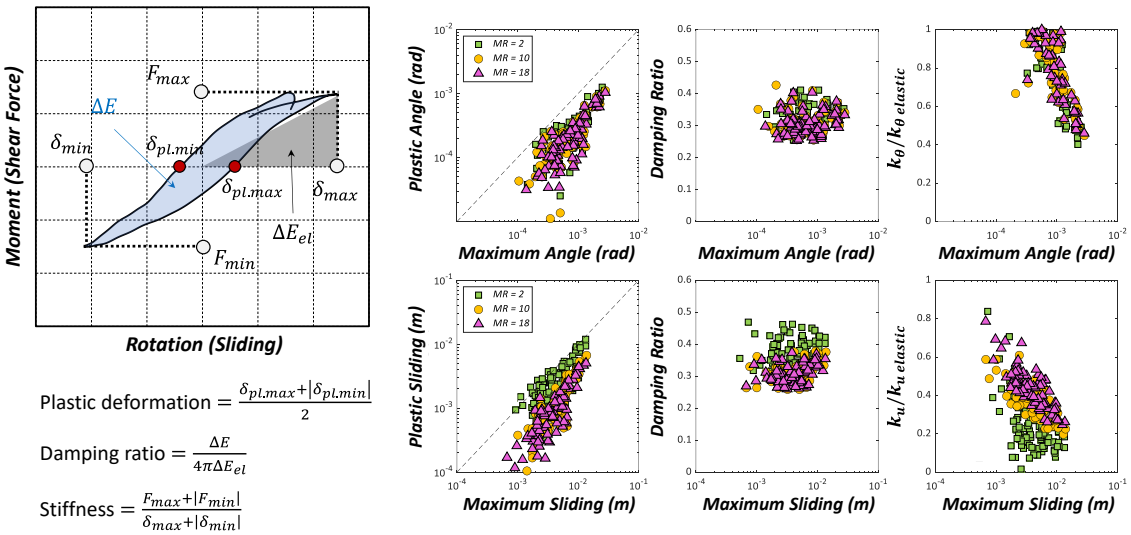

Fig. 10 Plastic deformation, damping ratio, and normalized stiffnesses with maximum deformation of each cycle for the rocking and sliding responses of the $FS_v = 3$ systems subjected to strong shaking (Ofunato, PGA at free-field soil surface: 0.78 g)

and FS3_MR18 under a strong earthquake (Ofunato, PGA at the free-field soil surface: 0.78 g). The plastic deformation increased with the maximum deformation, regardless of the sliding and rocking behaviors. The sliding (k_u) and rocking (k_θ) stiffnesses were normalized by the elastic stiffness of the embedded foundation (Stewart *et al.* 1999). The normalized stiffnesses for sliding and rocking decreased with the maximum deformation due to the nonlinear behavior of the foundation. The damping ratios for sliding and rocking were larger than 20%.

The rocking responses were independent of the *MR*, whereas the heavier foundation (FS3_MR2) exhibited a more significant damping and degradation of the stiffness with respect to the sliding responses. This indicates that the sliding response of a heavier foundation is induced by the inertia of the foundation, and not the structural inertial behavior. As Gajan and Kutter (2009) highlighted, given that the sliding behavior induces slightly more permanent settlement than the rocking behavior, a lower *MR* leads to larger settlement.

The displacement contour of the numerical model after the end of the shaking revealed the location of significant displacement (Fig. 11). Moreover, FS3_MR2 exhibited more sliding due to the inertia of the foundation, which consequently caused a differential settlement of the system (Fig. 11(a)). The shear stress distribution at the bottom of the foundation was concentrated primarily on one side of the foundation where sliding occurred. Conversely, for FS3_MR18 (the lighter foundation case), the displacement contour (Fig. 11(b)) indicated a seismic bearing capacity failure, as shown in Fig. 8. The permanent settlement exhibited a pattern of punching failure with even settlement around the foundation such that the stress distribution at the bottom of the foundation was even without tilting to one side.

The mean effective stress (p') and shear stress (q) curves at the soil 0.1 m below the foundation are shown in Fig. 11. The red and blue lines represent the responses of the soil below the edge of the foundation, and the green line represents the soil response below the middle of the foundation. The circle and triangle points indicate the values before and after shaking, respectively. Moreover, the $p'-q$ responses reached the failure line of the soil during the earthquake, regardless of the *MR*. As expected, the $p'-q$ responses of the soil located below the edges of the foundation were different for FS3_MR2 and similar for FS3_MR18. As an intermediate result, the sliding behavior of the foundation influenced and intensified the permanent settlement due to the foundation inertia of heavily-loaded systems.

4.4 Effect of MR for lightly-loaded systems: FS_v = 24

4.4.1 Response spectrum and settlement-rotation response

The lightly-loaded system introduces plastic hinge into the superstructure instead of the soil (Anastasopoulos *et al.* 2010). Therefore, the structural dynamic response requires investigation depending on the *MR*. For the heavier foundation case (FS24_MR2), the responses of the soil, foundation, and structure exhibited similar energies near 0.32 s (Fig. 12(a)). Conversely, for the lighter foundation case, the energies at 0.32 s differed between the soil, foundation, and structure systems (Fig. 12(b)). The structural natural periods of both systems were elongated more than those of the fixed-based conditions (0.4 s), and the period lengthening phenomenon of the structuredue to SFSI was more significant as the *MR* increased due to the considerable structural inertia. The impact of structural inertia was observed in the settlement–rotation responses. The structural inertial effect caused a dynamic foundation response. Accordingly, the rocking response and maximum dynamic rotation were significant for the case with the heavier structure and lighter foundation (FS24_MR18). However, the permanent settlements of the foundations were similar.

4.4.2 Foundation rocking and sliding responses

As shown in Fig. 13, the rocking and sliding hysteresis loops of the lightly-loaded systems were used to estimate the

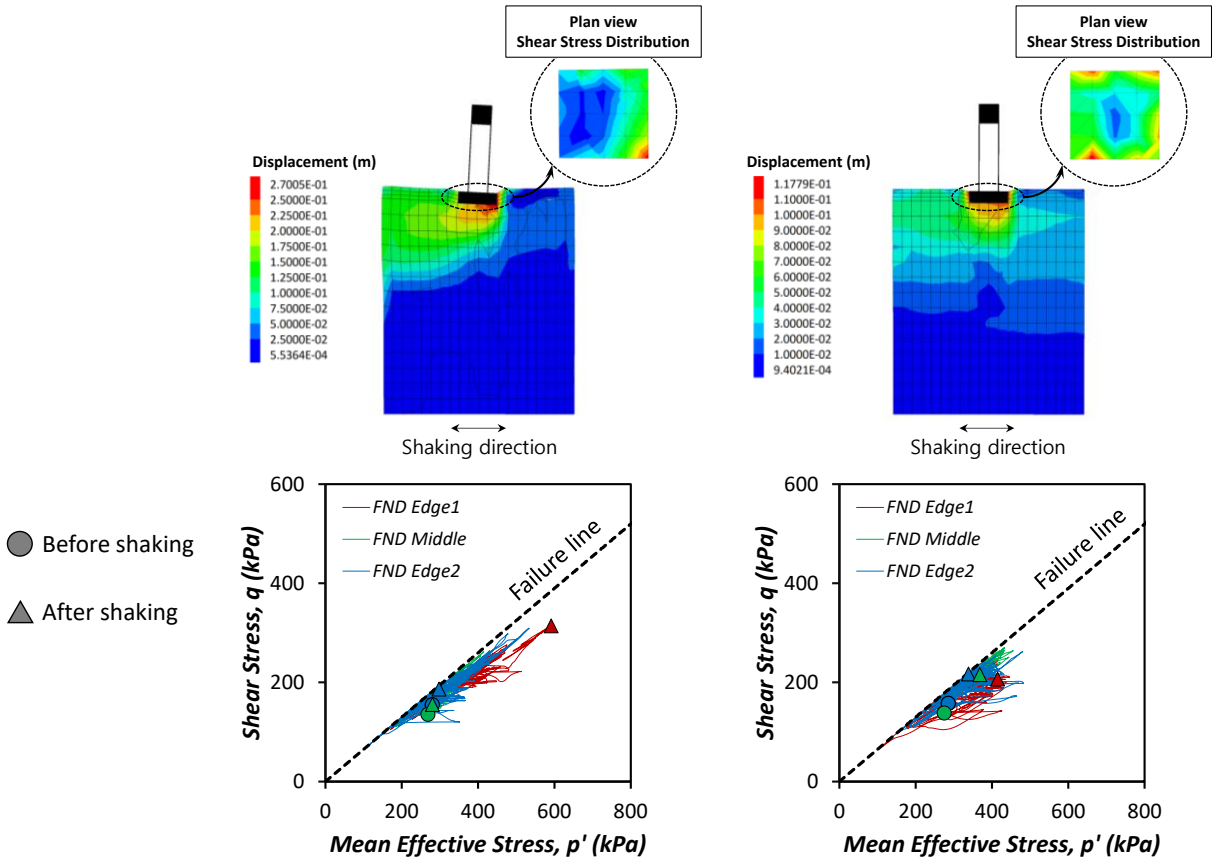

(a) FS3_MR2 (b) FS3_MR18

Fig. 11 Displacement contour of the numerical models, shear stress distributions on the foundation base after the shaking and mean effective stress (p') and shear stress (q) of the soil below the foundation (Ofunato, PGA at free-field soil surface: 0.78 g

plastic deformation, damping ratio, and normalized stiffness with maximum deformation under the Ofunato earthquake (PGA at the free-field soil surface: 0.39 g). It was observed that the *MR* for the lightly-loaded systems did not influence the sliding responses of the foundation, whereas the *MR* effects on sliding responses were observed for the heavily-loaded systems. However, the system with $MR = 2$ exhibited a slightly less plastic angle and degradation of the normalized rocking stiffness, which indicates that the case with the lighter structure and heavier foundation less stimulates the foundation rocking behavior relative to the case with the heavier structure and lighter foundation.

4.4.3 Time–frequency analysis: soil surface, foundation, and structure

The time–frequency domain (Figs. 14(a) and 14(b)) was obtained using the Stockwell transform, which exhibits a higher resolution in the time and frequency domains (Kramer *et al.* 2016). The foundation horizontal response ($\ddot{u}_f$) was in accordance with the frequency energy of free-field soil surface motion. The maximum structural acceleration ($\ddot{u}_s$) of the larger *MR* system with a heavier structure (Fig. 14(b)) was less than that of the smaller *MR* system with a lighter structure (Fig. 14(a)). The first was the rocking effect, which restricted structural seismic acceleration. As the structural inertia increased, the rocking behavior was dominant. The second was due to the elongation of the natural structural period. As exhibited in the time–frequency domains, the period-lengthening phenomenon was exhibited by the heavier structure model (FS24_MR18). Hence, the elongated structural period of FS24_MR18 avoided the primary frequency energy of soil surface motion. Consequently, with an increase in *MR*, the rocking behavior and period lengthening phenomena were more significant in the lightly-loaded system.

5. Conclusions

In this study, the influences of the structure-to-foundation *MR* on the seismic response and settlement of a foundation-structure system were investigated while considering the dynamic SFSI. The dynamic centrifuge test validated the 3D numerical model for the SFSI in terms of the acceleration records of the SFS system and the rotation–settlement behavior of the foundation. The validated numerical models were used for parametric analysis. The independent variables used herein were the *MR* and FS_v, and dimensionless parameters, such as the structural aspect ratio and soil-to-structure stiffness ratio, were fixed. The sensitivity study consisted of 54 cases with nine foundation-structure models depending on the *MR* and FS_v two different input motions, and three input peak accelerations. The findings are summarized below.

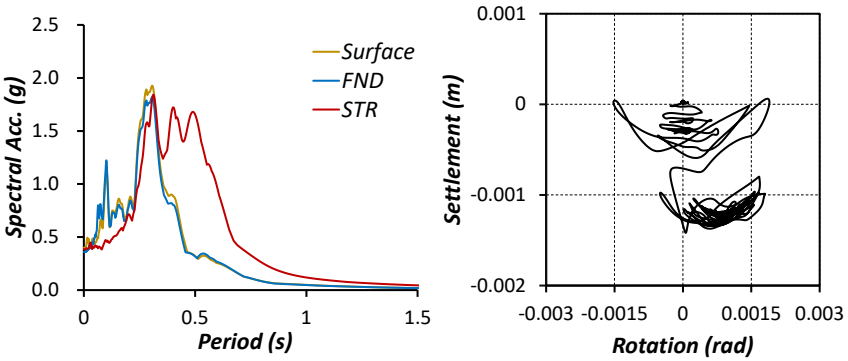

(a) FS24_MR2

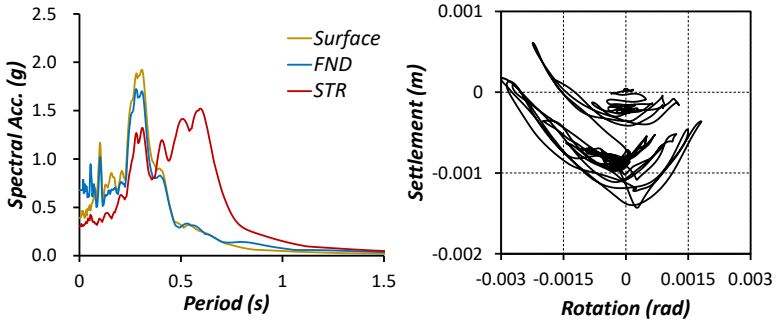

(b) FS24_MR18

Fig. 12 Dynamic responses of lightly loaded systems under the shaking (Ofunato, PGA at free-field soil surface: 0.39 g): acceleration response spectrum of soil-foundation-structure system and rotation-settlement behavior of the foundation

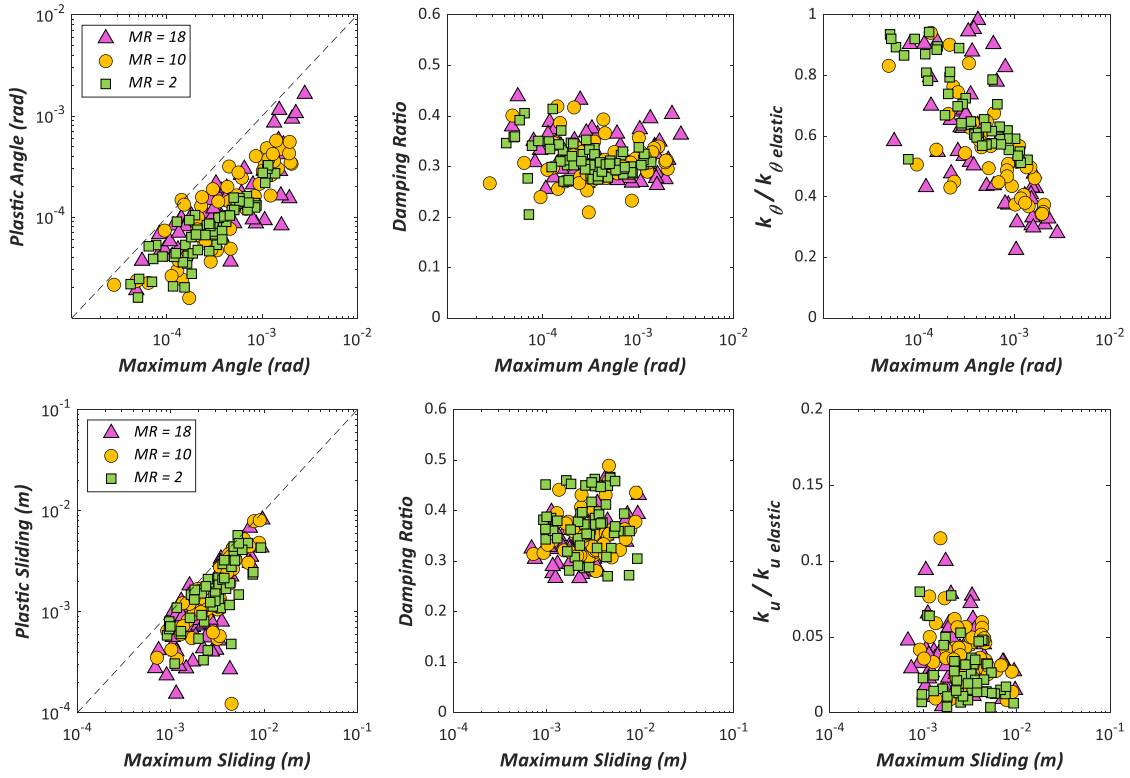

Fig. 13 Plastic deformation, damping ratio, and normalized stiffnesses with maximum deformation of each cycle for the rocking and sliding responses of $FS_v = 24$ systems subjected to the shaking (Ofunato, PGA at free-field soil surface: 0.39 g)

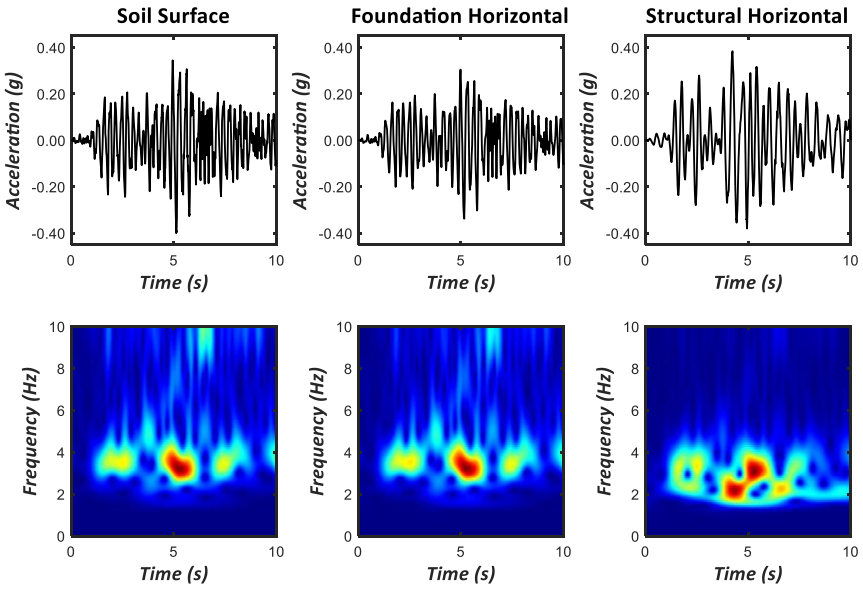

(a) FS24_MR2

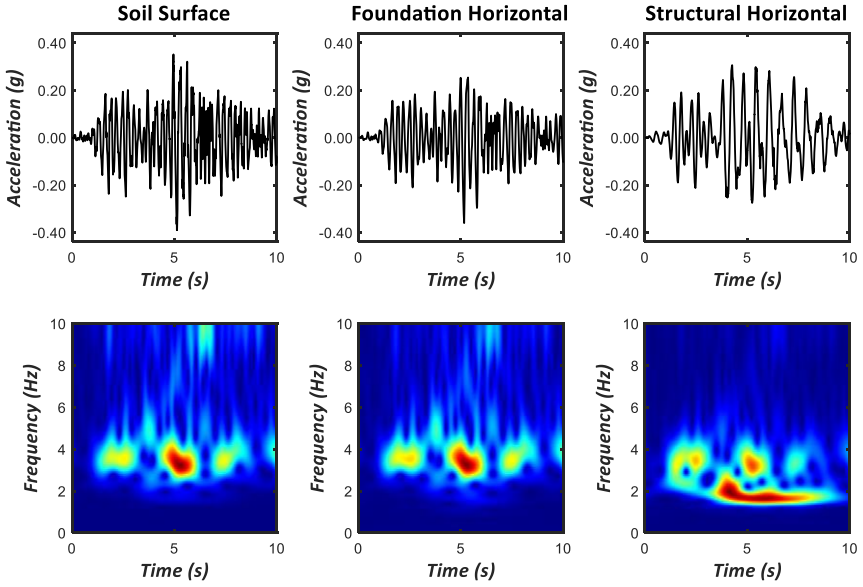

(b) FS24_MR18

Fig. 14 Acceleration time histories and time-frequency analysis of soil surface, foundation horizontal, and structural horizontal responses under the shaking (Ofunato, PGA at free-field soil surface: 0.39 g): (a) FS24_MR2 and (b) FS24_MR18

1. The SFSI effects reduced the structural seismic response and were more significant as the peak ground acceleration (PGA) at the free-field soil surface increased. Given that the heavily-loaded systems dissipated more seismic energy through the soil–foundation system than the superstructure, the heavily-loaded systems (low FS_v) exhibited a lower structural seismic response as compared with the lightly-loaded systems (high FS_v). For the same FS_v, it was found that with a decrease in the system *MR*, the seismic demand at the superstructure increased.
2. The permanent settlement and sliding of the foundation increased with the PGA at the free-field soil surface and the settlement was a function of FS_v. In contrast, when strong earthquakes were applied, the sliding of the foundation was associated with the *MR*. For the heavily-loaded systems, a more permanent settlement occurred in the lower *MR* systems. The *MR* of the system did not influence the foundation rocking behavior; however, it influenced the sliding behavior for lower FS_v systems. Sliding responses were found to pre-dominantly govern the foundation dynamic behavior for lower *MR*. Given that the foundation sliding behavior imposed additional shear stress on the soil below the foundation, the sliding responses due to the inertia of the heavier foundation intensified the permanent settlement.
3. For a lightly-loaded system (high FS_v), the structural inertia plays a critical role in the dynamic behavior of

the SFSI system. The foundation sliding responses were not influenced by the *MR* in the lightly-loaded systems. Systems with high *MR*s led to more structural dynamic motion, which caused a structural inertial effect on the foundation rocking behavior. Accordingly, the rocking behavior of the foundation was distinctly identified for the higher *MR* system, and more foundation rocking behavior generated a longer natural period of the superstructure due to SFSI effects. However, the influence of the *MR* on the permanent settlement of the system for the lightly-loaded systems was insignificant.

Acknowledgments

This research was supported by Korea Construction Engineering and Transport Development Collaboratory Management Institute (KOCED) and the National Research Foundation of Korea (NRF) grant funded by the Korea government (MSIT) (No. 2017R1A5A1014883).

References

Anastasopoulos, I., Gazetas, G., Loli, M., Apostolou, M. and Gerolymos, N. (2010), "Soil failure can be used for seismic protection of structures", *Bull. Earthq. Eng.*, **8**(2), 309-326. https://doi.org/10.1007/s10518-009-9145-2.

Cheney, R. and Chassie, R. (2000), *Soils and Foundations Workshop Reference Manual (No. FHWA NHI-00-045),* Washington, DC: Federal Highway Administration.

Chen, Z., Trombetta, N.W., Hutchinson, T.C., Mason, H.B., Bray, J.D. and Kutter, B.L. (2013), "Seismic system identification using centrifuge-based soil-structure interaction test data", *J. Earthq. Eng.*, **17**(4), 469-496. https://doi.org/10.1080/13632469.2012.762956.

Deviprasad, B.S. and Dodagoudar, G.R. (2020), "Seismic response of bridge pier supported on rocking shallow foundation", *Geomech. Eng.*, **21**(1), 73-84. https://doi.org/10.12989/gae.2020.21.1.073.

Gajan, S., Kutter, B.L., Phalen, J.D., Hutchinson, T.C. and Martin, G.R. (2005), "Centrifuge modeling of load-deformation behavior of rocking shallow foundations", *Soil Dyn. Earthq. Eng.*, **25**(7), 773-783. https://doi.org/10.1016/j.soildyn.2004.11.019.

Gajan, S. and Kutter, B.L. (2008), "Capacity, settlement, and energy dissipation of shallow footings subjected to rocking", *J. Geotech. Geoenviron. Eng.*, **134**(8), 1129-1141. https://doi.org/10.1061/(ASCE)1090-0241(2008)134:8(1129).

Gajan, S. and Kutter, B.L. (2009), "Effects of moment-to-shear ratio on combined cyclic load-displacement behavior of shallow foundations from centrifuge experiments", *J. Geotech. Geoenviron. Eng.*, **135**(8), 1044-1055. https://doi.org/10.1061/(ASCE)GT.1943-5606.0000034.

Gavras, A.G., Kutter, B.L., Hakhamaneshi, M., Gajan, S., Tsatsis, A., Sharma, K., Kohno, T., Deng, L., Anastasopoulos, I. and Gazetas, G. (2020), "Database of rocking shallow foundation performance: Dynamic shaking", *Earthq. Spectra*, **36**(2), 960-982. https://doi.org/10.1177/8755293019891727.

Ha, J.G., Ko, K.W., Jo, S.B., Park, H.J. and Kim, D.S. (2019), "Investigation of seismic performances of unconnected pile foundations using dynamic centrifuge tests", *Bull. Earthq. Eng.*, **17**(5), 2433-2458. https://doi.org/10.1007/s10518-018-00530-y.

Hardin, B.O. and Drnevich, V.P. (1972), "Shear modulus and damping in soils: Design equations and curves", *J. Soil Mech. Found. Div.*, **98**(7), 667-692. https://doi.org/10.1061/jsfeaq.0001760.

Huynh, V.Q., Nguyen, T.K. and Nguyen, X.H. (2021), "Seismic analysis of soil-structure interaction: experimentation and modeling", *Geomech. Eng.*, **27**(2), 115-121. https://doi.org/10.12989/gae.2021.27.2.115.

Itasca Consulting Group, Inc. (2019), FLAC3D — Fast Lagrangian Analysis of Continua in Three-Dimensions, Ver. 7.0. Minneapolis: Itasca.

Kimmerling, R.E., Bachus R.C., Mayne P.W., Scheider J.A. and Zettler T.E. (2002), *Geotechnical engineering circular no. 6, shallow foundations*, Washington, DC: Federal Highway Administration.

Kim, D.K., Lee, S., Kim, D., Choo, Y.W. and Park, H. (2015), "Rocking effect of a mat foundation on the earthquake response of structures", *J. Geotech. Geoenviron. Eng,* **141**(1), 04014085. https://doi.org/10.1061/(ASCE)GT.1943-5606.0001207

Ko, K.W., Ha, J.G. and Kim, D.S. (2020), "Structural inertial interaction effects on foundation behavior", *Soil Dyn. Earthq. Eng.*, **136**, 106238. https://doi.org/10.1016/j.soildyn.2020.106238.

Ko, K.W., Ha, J.G., Park, H.J. and Kim, D.S. (2021), "Investigation of period-lengthening ratio for single-degree-of-freedom structures using dynamic centrifuge test", *J. Earthq. Eng.*, **25**(7), 1358-1380. https://doi.org/10.1080/13632469.2019.1576557.

Kramer, S.L., Sideras, S.S. and Greenfield, M.W. (2016), "The timing of liquefaction and its utility in liquefaction hazard evaluation", *Soil Dyn. Earthq. Eng.*, **91**, 133-146. https://doi.org/10.1016/j.soildyn.2016.07.025.

Lee, S.H., Choo, Y.W. and Kim, D.S. (2013), "Performance of an equivalent shear beam (ESB) model container for dynamic geotechnical centrifuge tests", *Soil Dyn. Earthq. Eng.*, **44**, 102-114. https://doi.org/10.1016/j.soildyn.2012.09.008.

Lee, J.S., Chae, H.G., Kim, D.S., Jo, S.B. and Park, H.J. (2015), "Numerical analysis of inverted T-type wall under seismic loading", *Comput. Geotech.*, **66**, 85-95. https://doi.org/10.1016/j.compgeo.2015.01.013.

Lysmer, J. and Kuhlemeyer, R.L. (1969), "Finite dynamic model for infinite media", *J. Eng. Mech. Div.*, **95**(4), 859-877. https://doi.org/10.1061/JMCEA3.0001144.

Martakis, P., Taeseri, D., Chatzi, E. and Laue, J. (2017), "A centrifuge-based experimental verification of Soil-Structure Interaction effects", *Soil Dyn. Earthq. Eng.*, **103**, 1-14. https://doi.org/10.1016/j.soildyn.2017.09.005.

Meyerhof, G.G. (1963), "Some recent research on the bearing capacity of foundations", *Can. Geotech. J.*, **1**(1), 16-26. https://doi.org/10.1139/t63-003.

Mejía, L. and Dawson, E. (2006), *Earthquake deconvolution for FLAC*. In: de Varona, P., Hart, R.D., editors. FLAC and numerical modeling in geomechanics, *Proceedings of the 4th international FLAC symposium, 2006*, Madrid (Spain): Itasca Consulting Group.

Newmark, N.M. (1965), "Effects of earthquakes on dams and embankments", *Geotechnique*, **15**(2), 139-160. https://doi.org/10.1680/geot.1965.15.2.139.

Ngo, V.L., Kim, J.M. and Lee, C. (2019), "Influence of structure-soil-structure interaction on foundation behavior for two adjacent structures: Geo-centrifuge experiment", *Geomech. Eng.*, **19**(5), 407-420. https://doi.org/10.12989/gae.2019.19.5.407.

Raychowdhury, P. and Hutchinson, T.C. (2009), "Performance evaluation of a nonlinear Winkler-based shallow foundation model using centrifuge test results", *Earthq. Eng. Struct. Dyn.*, **38**(5), 679–698. https://doi.org/10.1002/eqe.902.

Richards, R., Elms, D.G. and Budhu, M. (1993), "Seismic bearing capacity and settlements of foundations", *J. Geotech. Eng.*, **119**(4), 662–674. https://doi.org/10.1061/(ASCE)0733-9410(1993)119:4(662).

Safak, E. (1995), "Detection and identification of soil-structure interaction in buildings from vibration recordings", *J. Struct. Eng.*, **121**(5), 899-906. https://doi.org/10.1061/(ASCE)0733-9445(1995)121:5(899).

Sbartai, B. (2020), "A polynomial mathematical tool for foundation-soil-foundation interaction", *Geomech. Eng.*, **23**(6), 547-560. https://doi.org/10.12989/gae.2020.23.6.547.

Schofield, A.N. (1980), "Cambridge geotechnical centrifuge operations", *Géotechnique*, **30**(3), 227-268. https://doi.org/10.1680/geot.1980.30.3.227.

Shirato, M., Kouno, T., Asai, R., Nakatani, S., Fukui, J. and Paolucci, R. (2008), "Large-scale experiments on nonlinear behavior of shallow foundations subjected to strong earthquakes", *Soils Found.*, **48**(5), 673-692. https://doi.org/10.3208/sandf.48.673.

Stewart, J.P., Fenves, G.L. and Seed, R.B. (1999), "Seismic soil-structure interaction in buildings. I: Analytical methods", *J. Geotech. Geoenviron. Eng.*, **125**(1), 26-37. https://doi.org/10.1061/(ASCE)1090-0241(1999)125:1(26).

Stewart, J.P. (2000), "Variations between foundation-level and free-field earthquake ground motions", *Earthq. Spectra*, **16**(2), 511-532. https://doi.org/10.1193/1.1586124.

Sun, Q. and Dias, D. (2018), "Significance of rayleigh damping in nonlinear numerical seismic analysis of tunnels", *Soil Dyn. Earthq. Eng.*, **115**, 489-494. https://doi.org/10.1016/j.soildyn.2018.09.013.

Tabatabaiefar, H.R. and Fatahi, B. (2014), "Idealisation of soil-structure system to determine inelastic seismic response of mid-rise building frames", *Soil Dyn. Earthq. Eng.*, **66**, 339-351. https://doi.org/10.1016/j.soildyn.2014.08.007.

Trifunac, M.D., Ivanović, S.S. and Todorovska, M.I. (2001), "Apparent periods of a building I: Fourier analysis", *J. Struct. Eng.*, **127**(5), 517-526. https://doi.org/10.1061/(ASCE)0733-9445(2001)127:5(517).

Yoo, M., Kwon, S.Y. and Hong, S. (2022). "Dynamic response evaluation of deep underground structures based on numerical simulation", *Geomech. Eng.*, **29**(3), 269-279. https://doi.org/10.12989/gae.2022.29.3.269.

Veletsos, A.S. and Meek, J.W. (1974), "Dynamic behaviour of building-foundation systems", *Earthq. Eng. Struct. Dyn.*, **3**(2), 121-138. https://doi.org/10.1002/eqe.4290030203.

Wolf, J. (1985), *Dynamic Soil-Structure Interaction*, Englewood Cliffs, NJ: PrenticeHall.

IC

Nomenclature

c_s	structural damping
f	the highest frequency of input wave
f_n	structural natural frequency
FSv	vertical factor of safety
F_h	shear force of the foundation
G	shear modulus within a small strain range of soil
h	structural height
k_h	critical acceleration
k_s	structural stiffness
k_u	foundation sliding stiffness
k_θ	foundation rocking stiffness
K	bulk modulus within a small strain range of soil
K_n	a linear spring in the normal direction
K_s	a spring-slider in the shear direction
L	foundation length
m_s	structural effective mass
m_f	foundation mass
MR	structure-to-foundation mass ratio (m_s/m_f)
M_o	overturning moment of the foundation
p'	mean effective stress of the soil
P_{AE}	active wedge angle of the simplified static slip field with Coulomb wedges
PGA	peak ground acceleration
q	shear stress of the soil
$\ddot{u}_f$	seismic acceleration of foundation
$\ddot{u}_g$	acceleration of free-field soil surface
$\ddot{u}_{net}$	seismic acceleration of the SDOF structure under fixed-base condition
$\ddot{u}_s$	structural seismic acceleration
V_s	shear wave velocity of soil
Δl	element size
ΔP_h	additional passive pressure
Δz_{min}	the smallest width of elements in normal direction
λ	wavelength of the highest frequency of input wave
σ	soil-to-structure stiffness ratio